JOURNAL OF THERMOPHYSICS AND HEAT TRANSFER
Vol. 18, No. 2, April–June 2004

Technical Notes

TECHNICAL NOTES are short manuscripts describing new developments or important results of a preliminary nature. These Notes cannot exceed six manuscript pages and three figures; a page of text may be substituted for a figure and vice versa. After informal review by the editors, they may be published within a few months of the date of receipt. Style requirements are the same as for regular contributions (see inside back cover).

Analytical Expressions for View Factors with an Intervening Surface

M. Deiveegan,* V. Ramamoorthy,*
and Subrahmanya S. Katte†
Shanmugha Arts, Science, Technology,
and Research Academy, Thanjavur 613 402, India

Nomenclature

A	=	finite area, m^2
dA_1	=	infinitesimally small element, m^2
F	=	view factor
L	=	distance between dA_1 and A_2, m
R	=	radius, m
S	=	distance between dA_1 to any point on A_2, m
x, y, z	=	Cartesian coordinates, m
$2W, 2B$	=	dimensions of rectangle, m
θ	=	angular coordinate measured from x axis in clockwise direction, rad
ξ_1, ξ_2	=	x and y coordinates of center of intervening surface respectively, m
ϕ	=	angular coordinate measured from x axis in anticlockwise direction, rad

Subscripts

2, 3, S	=	corresponding to finite areas A_2, A_3 and intervening surface A_S, respectively

Introduction

THE major obstacle in the thermal analysis of an enclosure containing objects is the determination of view factors accounting for shadowing effects because the integrations have to be carried out only over visible portions of the surfaces. Analytical expressions for view factors in the presence of intervening objects are available only for a few configurations.[1] There have been applications of the contour integration method[2] to account for the shadowing effect of base surface, while optimizing the space radiators.[3,4] Katte and Venkateshan[5] have provided analytical expressions for view factors for an axisymmetric enclosure with shadowing bodies inside, by application of the contour integration method. However, a review of the literature shows that expressions are not available for view factors between a coaxial differential element and a finite area, in the presence of a finite intervening surface. In the present work, expressions to this effect are developed using the contour integration method. The finite area and the intervening surfaces could be a circular disk or a rectangle, and the intervening surface could be at an arbitrary position.

Analysis

Consider the radiation between dA_1 and A_2, which is at distance of L from dA_1. The intervening surface A_S is located in between dA_1 and A_2, at unit distance from dA_1. Following Sparrow,[2] the coordinate system is chosen such that dA_1 lies at the origin, and hence, the view factor can be written as

$$2\pi F_{1d-2} = \oint_C \frac{(y_2\, dx_2 - x_2\, dy_2)}{S^2} \tag{1}$$

where $S^2 = x_2^2 + y_2^2 + z_2^2$. C represents the contour of visible portion of A_2 as seen from dA_1, on which z_2 remains constant during integration; the values of x_2 and y_2 vary. When the contour is subdivided, Cartesian and cylindrical coordinates are used for straight line and arc segments, respectively.

Four different combinations of geometries are considered, with several configurations depending on the dimensions and position of the intervening surface.

Case 1: View Factor Between dA_1 and Disk with a Disk in Between

Consider F_{1d-2} for the configuration shown in Figs. 1a and 1b. The coordinates of the center of the intervening disk A_S can be identified as (ξ_1, 0, 1). A_3 is the projected area of A_2 on the plane located at unit height from dA_1. When the solid angle is considered, F_{1d-2} in the presence of A_S will be same as the view factor between dA_1 and nonclipped area of A_3 by A_S (slightly shaded area in Fig. 1a, which is the contour). This contour is subdivided into two arcs: 1–2

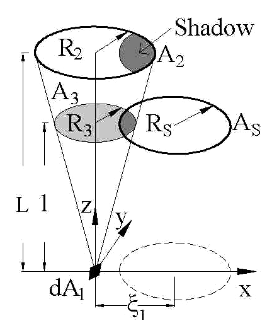

Fig. 1a Schematic of configuration 1a.

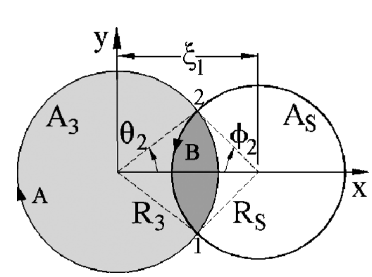

Fig. 1b Contour for configuration 1a.

Received 18 September 2003; revision received 9 October 2003; accepted for publication 11 October 2003.

*M. Tech Student, School of Mechanical Engineering, Tirumalaisamudram.

†Senior Lecturer, School of Mechanical Engineering, Tirumalaisamudram; sskatte@mech.sastra.edu.

along path A and 2–1 along path B and the direction of integration is shown in Fig. 1b.

When the arc 1–2 is considered, for any point on A_3, then $x_3 = R_3 \cos\theta$, $y_3 = R_3 \sin\theta$, $\mathrm{d}x_3 = -R_3 \sin\theta\, \mathrm{d}\theta$, and $\mathrm{d}y_3 = R_3 \cos\theta\, \mathrm{d}\theta$. The limit of integration θ varies from $(2\pi - \theta_2)$ to θ_2. On arc 2–1, $x_S = (\xi_1 - R_S \cos\phi)$, $y_S = R_S \sin\phi$, $\mathrm{d}x_S = R_S \sin\phi\, \mathrm{d}\phi$, and $\mathrm{d}y_S = R_S \cos\phi\, \mathrm{d}\phi$. The limit of integration ϕ varies from ϕ_2 to $-\phi_2$. From Fig. 1b, it can be shown that

$$\theta_2 = \cos^{-1}\left\{\frac{R_2^2 + L^2\left(\xi_1^2 - R_S^2\right)}{2R_2 L \xi_1}\right\}$$

$$\phi_2 = \cos^{-1}\left\{\frac{L^2\left(\xi_1^2 + R_S^2\right) - R_2^2}{2R_S L^2 \xi_1}\right\} \tag{2}$$

Substituting these, Eq. (1) becomes

$$2\pi F_{1d-2} = \int_{2\pi-\theta_2}^{\theta_2} \frac{-R_3^2 \sin^2\theta - R_3^2 \cos^2\theta}{R_3^2 \sin^2\theta + R_3^2 \cos^2\theta + 1}\, \mathrm{d}\theta + \int_{\phi_2}^{-\phi_2} \frac{R_S^2 \sin^2\phi + R_S^2 \cos^2\phi - \xi_1 R_S \cos\phi}{R_S^2 \sin^2\phi + (\xi_1 - R_S\cos\phi)^2 + 1}\, \mathrm{d}\phi \tag{3}$$

The integration can be carried out to obtain

$$2\pi F_{1d-2} = \frac{2\left(\xi_1^2 - R_S^2 + 1\right)}{\sqrt{\left(\xi_1^2 + R_S^2 + 1\right)^2 - 4\xi_1^2 R_S^2}} \tan^{-1} \times \left\{\frac{\tan(\phi_2/2)}{\sqrt{\left[1 + (\xi_1 - R_S)^2\right] \big/ \left[1 + (\xi_1 + R_S)^2\right]}}\right\} + \frac{2R_2^2}{R_2^2 + L^2}(\pi - \theta_2) - \phi_2 \tag{4}$$

If A_S is out side the solid angle subtended by A_3, $R_S \leq (\xi_1 - R_2/L)$, there is no shadowing effect on A_2, and Eq. (4) reduces to the form available in literature (configuration 14 in Ref. 1). If A_S shadows A_2 completely, $R_S \geq (\xi_1 + R_2/L)$, the view factor becomes zero.

Case 2: View Factors Between dA_1 and Disk with a Rectangle in Between

Consider F_{1d-2} for configuration 2a (Fig. 2a). The contour, the subdivisions, and the direction of integration are shown in Fig. 2b. On the arc A, $x_3 = R_3 \cos\theta$, $y_3 = R_3 \sin\theta$, $\mathrm{d}x_3 = -R_3 \sin\theta\, \mathrm{d}\theta$,

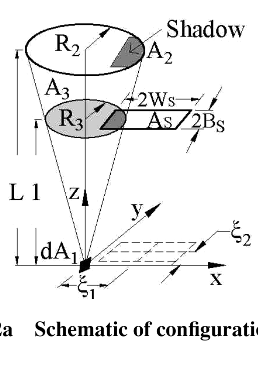

Fig. 2a Schematic of configuration 2a.

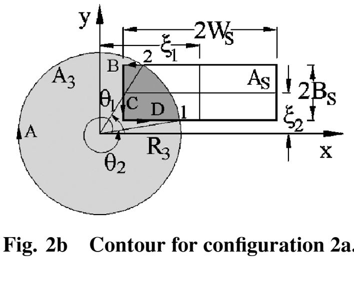

Fig. 2b Contour for configuration 2a.

and $\mathrm{d}y_3 = R_3 \cos\theta\, \mathrm{d}\theta$. The limit of integration θ varies from θ_2 to θ_1 where

$$\theta_1 = \sin^{-1}[L(\xi_2 + B_S)/R_2], \qquad \theta_2 = 2\pi + \sin^{-1}[L(\xi_2 - B_S)/R_2] \tag{5}$$

On line B, $y_S = (\xi_2 + B_S)$ remains constant, and $\mathrm{d}y_S = 0$ and x_S varies from $\sqrt{[R_3^2 - (\xi_2 + B_S)^2]}$ to $(\xi_1 - W_S)$. On line C, $x_S = (\xi_1 - W_S)$, $\mathrm{d}x_S = 0$, and y_S varies from $(\xi_2 + B_S)$ to $(\xi_2 - B_S)$. Finally, on line D, $y_S = (\xi_2 - B_S)$, $\mathrm{d}y_S = 0$, and x_S varies from $(\xi_1 - W_S)$ to $\sqrt{[R_3^2 - (\xi_2 - B_S)^2]}$. When these are substituted, Eq. (1) becomes

$$2\pi F_{1d-2} = \int_{\theta_2}^{\theta_1} \frac{-R_3^2}{R_3^2 + 1}\, \mathrm{d}\theta + \int_{\sqrt{R_3^2 - (\xi_2 + B_S)^2}}^{(\xi_1 - W_S)} \frac{\xi_2 + B_S}{x_3^2 + (\xi_2 + B_S)^2 + 1}\, \mathrm{d}x_3 + \int_{(\xi_2 + B_S)}^{(\xi_2 - B_S)} \frac{-(\xi_1 - W_S)}{(\xi_1 - W_S)^2 + y_3^2 + 1}\, \mathrm{d}y_3 + \int_{(\xi_1 - W_S)}^{\sqrt{R_3^2 - (\xi_2 - B_S)^2}} \frac{\xi_2 - B_S}{x_3^2 + (\xi_2 - B_S)^2 + 1}\, \mathrm{d}x_3 \tag{6}$$

Depending on the dimensions and position of A_S, five different configurations are possible under this case. For these configurations, expressions can be obtained following a similar procedure, which could be analytically integrated. For brevity, the closed-form solutions of five configurations are combined and given by

$$\begin{aligned} 2\pi F_{1d-2} = {} & \frac{R_2^2}{R_2^2 + L^2} C_1 + \frac{C_2}{\sqrt{C_2^2 + 1}} \left[\tan^{-1}\left(\frac{C_4}{\sqrt{C_2^2 + 1}}\right) - \tan^{-1}\left(\frac{\sqrt{R_2^2/L^2 - C_2^2}}{\sqrt{C_2^2 + 1}}\right) \right] \\ & + \frac{C_3}{\sqrt{C_3^2 + 1}} \left[\tan^{-1}\left(\frac{C_5}{\sqrt{C_3^2 + 1}}\right) - \tan^{-1}\left(\frac{\sqrt{R_2^2/L^2 - C_3^2}}{\sqrt{C_3^2 + 1}}\right) \right] \\ & + \frac{C_4}{\sqrt{C_4^2 + 1}} \left[\tan^{-1}\left(\frac{C_2}{\sqrt{C_4^2 + 1}}\right) - \tan^{-1}\left(\frac{C_5}{\sqrt{C_4^2 + 1}}\right) \right] \\ & + \frac{C_5}{\sqrt{C_5^2 + 1}} \left[\tan^{-1}\left(\frac{C_3}{\sqrt{C_5^2 + 1}}\right) - \tan^{-1}\left(\frac{C_4}{\sqrt{C_5^2 + 1}}\right) \right] \end{aligned} \tag{7}$$

The constants for different configurations are as follows.

For configuration 2a, valid for $|\xi_1 + R_2/L| \geq W_S \geq |\xi_1 - R_2/L|$, $B_S \leq |\xi_2 - R_2/L|$, and $B_S \leq |\xi_2 + R_2/L|$,

$$C_1 = 2\pi + \sin^{-1}[L(\xi_2 - B_S)/R_2] - \sin^{-1}[L(\xi_2 + B_S)/R_2]$$

$$C_2 = \xi_2 + B_S, \qquad C_3 = \sqrt{R_2^2/L^2 - (\xi_2 - B_S)^2}$$

$$C_4 = \xi_1 - W_S, \qquad C_5 = \xi_2 - B_S$$

For configuration 2b, valid for $|\xi_1 + R_2/L| \geq W_S \geq |\xi_1 - R_2/L|$ and $|\xi_2 - R_2/L| \leq B_S \leq |\xi_2 + R_2/L|$,

$$C_1 = 2\pi + \sin^{-1}[L(\xi_2 - B_S)/R_2] - \cos^{-1}[L(\xi_2 - W_S)/R_2]$$

$$C_2 = \sqrt{R_2^2 \big/ L^2 - (\xi_1 - W_S)^2}, \qquad C_3 = \sqrt{R_2^2 \big/ L^2 - (\xi_2 - B_S)^2}$$

$$C_4 = \xi_1 - W_S, \qquad C_5 = \xi_2 - B_S$$

For configuration 2c, valid for $|\xi_1 + R_2/L| \geq W_S \geq |\xi_1 - R_2/L|$, $B_S \geq |\xi_2 - R_2/L|$, and $B_S \geq |\xi_2 + R_2/L|$,

$$C_1 = 2\pi - 2\cos^{-1}[L(\xi_2 - W_S)/R_2], \qquad C_2 = -(\xi_1 - W_S)$$

$$C_3 = -(\xi_1 - W_S), \qquad C_4 = 0, \qquad C_5 = 0$$

For configuration 2d, valid for $|\xi_1 + R_2/L| \geq W_S \geq |\xi_1 - R_2/L|$, $B_S \leq |\xi_2 - R_2/L|$, and $B_S \leq |\xi_2 + R_2/L|$,

$$C_1 = 2\pi + \cos^{-1}[L(\xi_1 + W_S)/R_2] - \sin^{-1}[L(\xi_2 + B_S)/R_2]$$

$$C_2 = \xi_2 + B_S, \qquad C_3 = \xi_1 + W_S$$

$$C_4 = \xi_1 - W_S, \qquad C_5 = \xi_2 - B_S$$

For configuration 2e, valid for $W_s \geq |\xi_1 + R_2/L|$, $W_S \geq |\xi_1 - R_2/L|$, $B_S \leq |\xi_2 - R_2/L|$, and $B_S \leq |\xi_2 + R_2/L|$,

$$C_1 = 2\pi + 2\sin^{-1}[L(\xi_2 - B_S)/R_2] - 2\sin^{-1}[L(\xi_2 + B_S)/R_2]$$

$$C_2 = -(\xi_2 + B_S), \qquad C_3 = -(\xi_2 + B_S)$$

$$C_4 = 0, \qquad C_5 = 0$$

For configuration 2a, if there is no intervening rectangle, by the substitution of $2W_S = 2B_S = 0$, Eq. (7) reduces to the form available in literature (configuration 14 in Ref. 1). If A_S is shadowing exactly half of A_2, that is, $\xi_1 = W_S$, $\xi_2 = 0$, and $B_S = R_2/L$, then Eq. (7) reduces to the form $F_{1d-2} = R_2^2/[2(R_2^2 + L^2)]$, which is the view factor from dA_1 to a semicircular disk.

Case 3: View Factors Between dA_1 and Rectangle with a Rectangle in Between

Consider F_{1d-2} for configuration 3a (Fig. 3a). The contour, the subdivisions, and the direction of integration are shown in Fig. 3b. On line A, $x_3 = W_3$, $dx_3 = 0$, and y_3 varies from $(\xi_2 - B_S)$ to $-B_3$. On line B, $y_3 = -B_3$, $dy_3 = 0$, and x_3 varies from W_3 to $-W_3$. On line C, $x_3 = -W_3$, $dx_3 = 0$, and y_3 varies from $-B_3$ to B_3. On line D, $y_3 = B_3$, $dy_3 = 0$, and x_3 varies from $-W_3$ to W_3. On line E, $x_3 = W_3$, $dx_3 = 0$, and y_3 varies from B_3 to $(\xi_2 + B_S)$. On line F, $y_S = (\xi_2 + B_S)$, $dy_S = 0$, and x_S varies from W_3 to $(\xi_1 - W_S)$. On line G, $x_S = (\xi_1 - W_S)$, $dx_S = 0$, and y_S varies from $(\xi_2 + B_S)$ to $(\xi_2 - B_S)$. Finally, on line H, $y_S = (\xi_2 - B_S)$, $dy_S = 0$, and x_S varies from $(\xi_1 - W_S)$ to W_S. When these are substituted, Eq. (1) becomes

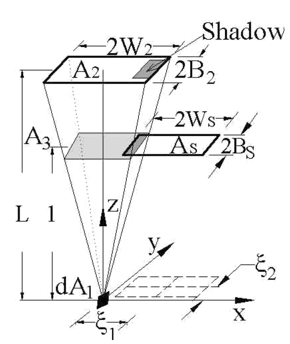

Fig. 3a Schematic of configuration 3a.

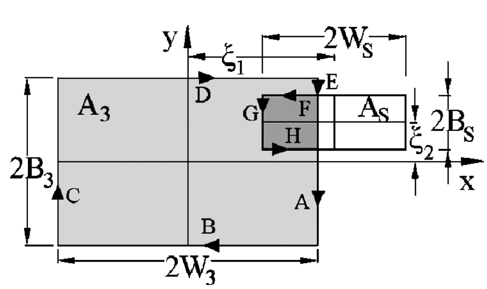

Fig. 3b Contour for configuration 3a.

$$\begin{aligned}
2\pi F_{1d-2} = {} & \int_{(\xi_2 - B_S)}^{-B_3} \frac{-W_3}{W_3^2 + y_3^2 + 1}\, dy_3 + \int_{W_3}^{-W_3} \frac{-B_3}{x_3^2 + B_3^2 + 1}\, dx_3 \\
& + \int_{-B_3}^{B_3} \frac{W_3}{W_3^2 + y_3^2 + 1}\, dy_3 + \int_{-W_3}^{W_3} \frac{B_3}{x_3^2 + B_3^2 + 1}\, dx_3 \\
& + \int_{B_3}^{(\xi_2 + B_S)} \frac{-W_3}{W_3^2 + y_3^2 + 1}\, dy_3 \\
& + \int_{W_3}^{(\xi_1 - W_S)} \frac{\xi_2 + B_S}{x_3^2 + (\xi_2 + B_S)^2 + 1}\, dx_3 \\
& + \int_{(\xi_2 + B_S)}^{(\xi_2 - B_S)} \frac{-(\xi_1 - W_S)}{(\xi_1 - W_S)^2 + y_3^2 + 1}\, dy_3 \\
& + \int_{(\xi_1 - W_S)}^{W_3} \frac{\xi_2 - B_S}{x_3^2 + (\xi_2 - B_S)^2 + 1}\, dx_3
\end{aligned} \tag{8}$$

Here, four different configurations are possible, and the combined solution is

$$\begin{aligned}
2\pi F_{1d-2} = {} & \frac{4W_2}{\sqrt{W_2^2 + L^2}} \tan^{-1}\left(\frac{B_2}{\sqrt{W_2^2 + L^2}}\right) \\
& + \frac{4B_2}{\sqrt{B_2^2 + L^2}} \tan^{-1}\left(\frac{W_2}{\sqrt{B_2^2 + L^2}}\right) \\
& + \frac{W_2}{\sqrt{W_2^2 + L^2}} \left[\tan^{-1}\left(\frac{C_4 L}{\sqrt{W_2^2 + L^2}}\right) \right. \\
& \left. - \tan^{-1}\left(\frac{C_3 L}{\sqrt{W_2^2 + L^2}}\right)\right] \\
& + \frac{C_2}{\sqrt{C_2^2 + 1}} \left[\tan^{-1}\left(\frac{C_3}{\sqrt{C_2^2 + 1}}\right) - \tan^{-1}\left(\frac{C_4}{\sqrt{C_2^2 + 1}}\right)\right] \\
& + \frac{C_3}{\sqrt{C_3^2 + 1}} \left[\tan^{-1}\left(\frac{C_2}{\sqrt{C_3^2 + 1}}\right) - \tan^{-1}\left(\frac{W_2/L}{\sqrt{C_3^2 + 1}}\right)\right] \\
& + \frac{C_4}{\sqrt{C_4^2 + 1}} \left[\tan^{-1}\left(\frac{W_2/L}{\sqrt{C_4^2 + 1}}\right) - \tan^{-1}\left(\frac{C_2}{\sqrt{C_4^2 + 1}}\right)\right]
\end{aligned} \tag{9}$$

The constants for different configurations are as follows.

For configuration 3a, valid for $|\xi_1 + W_2/L| \geq W_S \geq |\xi_1 - W_2/L|$, $B_S \leq |\xi_2 - B_2/L|$, and $B_S \leq |\xi_2 + B_2/L|$,

$$C_2 = (\xi_1 - W_S), \qquad C_3 = (\xi_2 + B_S), \qquad C_4 = (\xi_2 - B_S)$$

For configuration 3b, valid for $|\xi_1 + W_2/L| \geq W_S \geq |\xi_1 - W_2/L|$, and $|\xi_2 + B_2/L| \geq B_S \geq |\xi_2 - B_2/L|$,

$$C_2 = (\xi_1 - W_S), \qquad C_3 = B_2/L, \qquad C_4 = (\xi_2 - B_S)$$

For configuration 3c, valid for $|\xi_1 + W_2/L| \geq W_S \geq |\xi_1 - W_2/L|$, $B_S \geq |\xi_2 - B_2/L|$, and $B_S \geq |\xi_2 + B_2/L|$,

$$C_2 = (\xi_1 - W_S), \qquad C_3 = B_2/L, \qquad C_4 = -B_2/L$$

For configuration 3d, valid for $W_S \geq |\xi_1 + W_2/L|$, $W_S \geq |\xi_1 - W_2/L|$, $B_S \leq |\xi_2 - B_2/L|$, and $B_S \leq |\xi_2 + B_2/L|$,

$$C_2 = -W_2/L, \qquad C_3 = (\xi_2 + B_S), \qquad C_4 = (\xi_2 - B_S)$$

For configurations 3a, if there is no intervening rectangle, $2W_S = 2B_S = 0$, Eq. (9) reduces to the form available in literature (configuration 4, in Ref. 1). For $W_S = \xi_1 + W_2/L$, $\xi_2 = 0$, and $B_S = B_2/L$, the intervening rectangle shadows A_2 completely, and the view factor becomes zero.

Case 4: View Factors Between dA_1 and Rectangle with Disk in Between

Consider F_{1d-2} for configuration 4a (Fig. 4a). The contour, the subdivisions and the direction of integration are shown in Fig. 4b. On line A, $x_3 = W_3$, $dx_3 = 0$, and y_3 varies from $(\xi_2 - \sqrt{[R_S^2 - (\xi_1 - W_3)^2]})$ to $-B_3$. On line B, $y_3 = -B_3$, $dy_3 = 0$, and x_3 varies from W_3 to $-W_3$. On line C, $x_3 = -W_3$, $dx_3 = 0$, and y_3 lies from $-B_3$ to B_3. On line D, $y_3 = B_3$, $dy_3 = 0$, and x_3 varies from $-W_3$ to W_3. On line E, $x_3 = W_3$, $dx_3 = 0$, and y_3 varies from B_3 to $(\xi_2 + \sqrt{[R_S^2 - (\xi_1 - W_3)^2]})$. Finally on the arc F, $x_S = \xi_1 + R_S \cos\theta$ and $y_S = \xi_2 + R_S \sin\theta$ and $dx_S = -R_S \sin\theta \, d\theta$ and $dy_S = R_S \cos\theta \, d\theta$. The limit of integration θ varies from θ_1 to θ_2, where

$$\theta_1 = \pi - \cos^{-1}[(\xi_1 - W_2/L)/R_S]$$

$$\theta_2 = \pi + \cos^{-1}[(\xi_1 - W_2/L)R_S] \tag{10}$$

When these are substituted, Eq. (1) becomes

$$\begin{aligned} 2\pi F_{1d-2} = & \int_{\left[\xi_2 - \sqrt{R_S^2 - (\xi_1 - W_3)^2}\right]}^{-B_3} \frac{-W_3}{W_3^2 + y_3^2 + 1} \, dy_3 \\ & + \int_{W_3}^{-W_3} \frac{-B_3}{x_3^2 + B_3^2 + 1} \, dx_3 + \int_{-B_3}^{B_3} \frac{W_3}{W_3^2 + y_3^2 + 1} \, dy_3 \\ & + \int_{-W_3}^{W_3} \frac{B_3}{x_3^2 + B_3^2 + 1} \, dx_3 \\ & + \int_{B_3}^{\left[\xi_2 + \sqrt{R_S^2 - (\xi_1 - W_3)^2}\right]} \frac{-W_3}{W_3^2 + y_3^2 + 1} \, dy_3 \\ & + \int_{\theta_1}^{\theta_2} \frac{(\xi_2 + R_S \sin\theta)(-R_S \sin\theta) - (\xi_1 + R_S \cos\theta)(R_S \cos\theta)}{\left[1 + \xi_1^2 + \xi_2^2 + R_S^2 + 2R_S(\xi_1 \cos\theta + \xi_2 \sin\theta)\right]} \, d\theta \end{aligned} \tag{11}$$

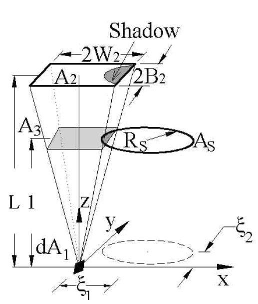

Fig. 4a Schematic of configuration 4a.

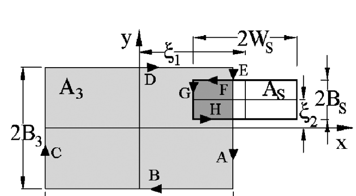

Fig. 4b Contour for configuration 4a.

Here, four different configurations are possible and the combined solution is

$$\begin{aligned} 2\pi F_{1d-2} = & \frac{C_1 W_2}{\sqrt{W_2^2 + L^2}} \tan^{-1}\left(\frac{B_2}{\sqrt{W_2^2 + L^2}}\right) \\ & + \frac{C_1 B_2}{\sqrt{B_2^2 + L^2}} \tan^{-1}\left(\frac{W_2}{\sqrt{B_2^2 + L^2}}\right) \\ & + \frac{C_2}{\sqrt{C_2^2 + 1}} \tan^{-1}\left(\frac{C_4}{\sqrt{C_2^2 + 1}}\right) \\ & + \frac{C_3}{\sqrt{C_3^2 + 1}} \tan^{-1}\left(\frac{C_5}{\sqrt{C_3^2 + 1}}\right) + \left(\frac{\theta_1 - \theta_2}{2}\right) \\ & + \frac{t}{\sqrt{r^2 - p^2 - q^2}} \left\{ \tan^{-1}\left[\frac{p + (r - q)\tan(\theta_2/2)}{\sqrt{r^2 - p^2 - q^2}}\right] \right. \\ & \left. - \tan^{-1}\left[\frac{p + (r - q)\tan(\theta_1/2)}{\sqrt{r^2 - p^2 - q^2}}\right] \right\} \end{aligned} \tag{12}$$

where $t = 1 - R^2 + \xi_1^2 + \xi_2^2$, $r = 1 + R^2 + \xi_1^2 + \xi_2^2$, $p = 2R_S\xi_2$, and $q = 2R_S\xi_1$, and the constants for different configurations are as follows.

For configuration 4a, valid for $|\xi_1 + W_2/L| \geq R_S \geq |\xi_1 - W_2/L|$, $R_S \leq |\xi_2 + B_2/L|$, and $R_S \leq |\xi_2 - B_2/L|$,

$$C_1 = 4, \qquad C_2 = W_2/L, \qquad C_3 = -W_2/L$$

$$C_4 = \xi_2 - \sqrt{R_S^2 - (\xi_1 - W_2/L)^2}$$

$$C_5 = \xi_2 + \sqrt{R_S^2 - (\xi_1 - W_2/L)^2}$$

$$\theta_1 = \pi - \cos^{-1}[(\xi_2 - W_2/L)/R_S]$$

$$\theta_2 = \pi + \cos^{-1}[(\xi_2 - W_2/L)/R_S]$$

For configuration 4b, valid for $|\xi_1 + W_2/L| \geq R_S \geq |\xi_1 - W_2/L|$ and $|\xi_2 + B_2/L| \geq R_S \geq |\xi_2 - B_2/L|$,

$$C_1 = 3, \qquad C_2 = B_2/L, \qquad C_3 = W_2/L$$

$$C_4 = \xi_1 - \sqrt{R_S^2 - (\xi_2 - B_2/L)^2}$$

$$C_5 = \xi_2 - \sqrt{R_S^2 - (\xi_1 - W_2/L)^2}$$

$$\theta_1 = \pi + \sin^{-1}[(\xi_2 - B_2/L)/R_S]$$

$$\theta_2 = \pi + \cos^{-1}[(\xi_2 - W_2/L)/R_S]$$

For configuration 4c, valid for $|\xi_1 + W_2/L| \geq R_S \geq |\xi_1 - W_2/L|$, $R_S \geq |\xi_2 + B_2/L|$, and $R_S \geq |\xi_2 - B_2/L|$,

$$C_1 = 2, \qquad C_2 = B_2/L, \qquad C_3 = B_2/L$$

$$C_4 = \xi_1 - \sqrt{R_S^2 - (\xi_2 - B_2/L)^2}$$

$$C_5 = \xi_1 - \sqrt{R_S^2 - (\xi_2 + B_2/L)^2}$$

$$\theta_1 = \pi + \sin^{-1}[(\xi_2 - B_2/L)/R_S]$$

$$\theta_2 = \pi + \sin^{-1}[(\xi_2 + B_2/L)R_S]$$

For configuration 4d, valid for $R_S \geq |\xi_1 + W_2/L|$, $R_S \geq |\xi_1 - W_2/L|$, $R_S \geq |\xi_2 + B_2/L|$, and $R_S \geq |\xi_2 - B_2/L|$,

$$C_1 = 1, \qquad C_2 = B_2/L, \qquad C_3 = W_2/L$$

$$C_4 = \xi_2 - \sqrt{R_S^2 - (\xi_1 + W_2/L)^2}$$

$$C_5 = \xi_1 - \sqrt{R_S^2 - (\xi_2 + B_2/L)^2}$$

$$\theta_1 = \pi + \cos^{-1}[(\xi_2 + W_2/L)/R_S]$$

$$\theta_2 = \pi + \sin^{-1}[(\xi_2 + B_2/L)/R_S]$$

For configuration 4a, for $R_S \leq (\xi_1 - W_2/L)$, no shadowing effect will be there, the view factor expression reduces to the form available in literature (configuration 4 in Ref. 1).

Conclusions

Closed-form solutions are presented for the view factors between a coaxial differential element and a finite area, when an intervening finite area at an arbitrary position is present in between. Four totally different combinations of geometrics are considered and the finite areas could be either a circular disk or a rectangle. Depending on the position and dimensions of the intervening surface, analytical expressions have been presented for a total of 14 configurations. When the intervening surface is not present and/or when it has particular dimensions and positions, the expressions presented reduce to the form available in literature.

References

[1]Siegel, R., and Howell, J. R., *Thermal Radiation Heat Transfer,* 3rd ed., Taylor and Francis, Washington, DC, 1972, Appendix C.

[2]Sparrow, E. M., "A New and Simpler Formulation of Radiative Angle Factors," *Journal of Heat Transfer,* Vol. 85, No. 2, 1963, pp. 81–88.

[3]Sunil Kumar, S., and Venkateshan, S. P., "Optimized Tubular Radiator with Annular Fins on a Non-Isothermal Base," *International Journal of Heat and Fluid Flow*, Vol. 15, No. 5, 1994, pp. 399–409.

[4]Ramesh, N., and Venkateshan, S. P., "Optimum Finned Tubular Space Radiator," *Heat Transfer Engineering*, Vol. 18, No. 4, 1997, pp. 69–87.

[5]Katte, S. S., and Venkateshan, S. P., "Accurate Determination of View Factors in Axisymmetric Enclosures with Shadowing Bodies Inside," *Journal of Thermophysics and Heat Transfer*, Vol. 14, No. 1, 2000, pp. 68–76.

One-Dimensional Analysis of Hollow Conical Radiating Fin

M. Deiveegan* and Subrahmanya S. Katte†
Shanmugha Arts, Science, Technology, and Research Academy, Thanjavur 613 402, India

Nomenclature

H, R, t	=	height, radius, and thickness of the fin, m
J	=	radiosity, W/m^2
k	=	thermal conductivity, W/m K
Q	=	rate of heat loss, W
T	=	temperature, K
ε	=	emissivity
θ	=	fin angle, rad
ρ	=	density, kg/m^3
σ	=	Stefan–Boltzman constant

Subscripts

e	=	corresponds to space
I, O	=	correspond to inside and outside fin surfaces
im	=	improvement per unit mass
UB	=	corresponds to unfinned isothermal base

Received 16 October 2003; revision received 4 November 2003; accepted for publication 4 November 2003.

*M.Tech Student, Tirumalaisamudram.

†Senior Lecturer, School of Mechanical Engineering, Tirumalaisamudram; sskatte@mech.sastra.edu.

Introduction

BECAUSE the mass is at a premium on spacecraft, several researchers[1–6] have attempted to optimize the finned space radiators used for waste heat rejection. Bhise et al.[7] investigated a corrugated structure in this regard. Srinivasan and Katte[8] proposed a grooved radiator with higher heat loss per unit mass compared to the flat radiator. A literature review shows that there are only a few attempts to modify the configuration while optimizing the radiating fins. Presently, a hollow conical configuration for radiating fin is proposed to augment the heat loss per unit mass. A one-dimensional analysis of such a fin is carried out. Effects of various parameters are studied and correlations are presented for optimum parameters.

Analysis

The hollow conical fin (Fig. 1) radiates heat from inside, outside, and tip surfaces in addition to the base surface, which is assumed to be maintained at T_B. The assumptions are as follows: the heat conduction is one dimensional along the axis, all of the surfaces are diffuse and gray, and the space is a black surface at T_e. Radiosity-irradiation method is used to account for the fin-base interaction and the interaction among the fin enclosure itself. As a conservative approach to account for the fin-base interaction, R_B is taken as twice R_T for $\theta = 10$ deg.

For the differential element (Fig. 1), the energy balance equation can be shown to be

$$\frac{\mathrm{d}}{\mathrm{d}x}\left(r\frac{\mathrm{d}T}{\mathrm{d}x}\right) + \frac{r}{kt\sin\theta}\frac{\varepsilon}{(1-\varepsilon)}\left(\sigma T^4 - J_I\right)\mathrm{d}x + \frac{r}{kt\sin\theta}\frac{\varepsilon}{(1-\varepsilon)}\left(\sigma T^4 - J_O\right)\mathrm{d}x = 0 \tag{1}$$

with boundary conditions

$$T(x=0) = T_B \qquad \text{and} \qquad \left.\frac{\mathrm{d}T}{\mathrm{d}x}\right|_{(x=H)} = \frac{-\sigma\varepsilon}{k}\left(T^4 - T_e^4\right)\Big|_{(x=H)}$$

The view factors for inside and outside surfaces are calculated using expressions for parallel coaxial disks of unequal radii (configuration C-41),[9] annular disk to coaxial truncated cone (configuration C-49), and view factor algebra. Because the temperatures and radiosities are coupled, an iterative method, in general, is used. Based on the assumed temperatures, the radiosities are calculated using the Gauss–Seidel technique for each enclosure. Using these radiosities, the nodal temperatures are calculated by solving Eq. (1) in the finite difference form using tridiagonal matrix algorithm, after linearization. The iterations are repeated until the temperatures are converged. The heat loss Q and improvement in heat loss per unit mass over the unfinned base surface $Q_{\mathrm{im}} = (Q - Q_{\mathrm{UB}})/m$ are calculated, where m is the mass of fin.

Results and Discussion

For all of the cases, the parameters considered are $T_B = 313$ K, $T_e = 4$ K, and $k = 177$ W/m K, and grid sensitivity studies are carried

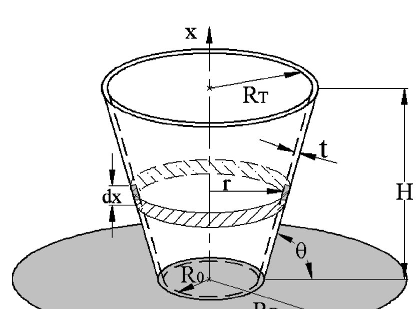

Fig. 1 Schematic of hollow conical radiating fin.